Am J Transl Res 2026;18(6):5145-5164
www.ajtr.org /ISSN:1943-8141/AJTR0168111

Original Article

Psoralen regulates bone degenerative diseases by inhibiting APP phosphorylation to regulate MAPK and STAT3 signaling

Youji Jia[1], Wei Yan[1], Tao Liu[1], Yong Xu[1,2], Zhongwei Li[1], Xiaobing Xi[1,2]

[1]Department of Traumatology, Shanghai Ruijin Hospital, Shanghai Jiao Tong University School of Medicine, Shanghai 200025, China; [2]Shanghai Key Laboratory for Bone and Joint Diseases, Shanghai Institute of Traumatology and Orthopaedics, Shanghai Ruijin Hospital, Shanghai Jiao Tong University School of Medicine, Shanghai 200025, China

Received August 14, 2025; Accepted May 15, 2026; Epub June 15, 2026; Published June 30, 2026

Abstract: Background: Psoralen can modulate bone metabolism pathways. This study investigated its effects on bone degenerative diseases, amyloid precursor protein (APP) phosphorylation, and the related pathways. Methods: The Aβ40/Aβ42 levels in mouse serum were analyzed through enzyme-linked immunosorbent assay (ELISA) across ages. mRNA levels of APP, APH-1α, PEN-2, and RAGE were determined through polymerase chain reaction (PCR). Thereafter, three degenerative models, including knee osteoarthritis, osteoporosis, and intervertebral disc degeneration, were established. Mice with APP knockout were generated, and the pathology was evaluated at weeks 4-20 through safranin O staining, osteoclast counting (immunohistochemistry, IHC), and hematoxylin and eosin (H&E) staining. Subsequently, TNF-α and HA contents were examined by ELISA, and Col2 expression and apoptosis were also analyzed. Furthermore, the anti-osteoporotic mechanisms of psoralen were explored at the cellular and animal levels. Results: As the mice aged, the expression of p-APP increased significantly, while that of proteins involved in the pathway decreased markedly. By constructing an APP knockout mouse model, it was found that after APP knockout, the mice developed bone degenerative lesions, which intensified with age. Intervention with psoralen was effective for ameliorating the pathologic condition of bone degenerative lesions in mice, and inhibiting the progression of bone tissue pathology. Notably, this effect exhibited a dose-dependent trend. Besides, intervention with psoralen in osteoblasts promoted osteoblast proliferation and regulated the phosphorylation of MAPK, AKT, and STAT3. For osteoblasts treated with pathway inhibitors and psoralen, psoralen exerted its effects through the MAPK, AKT, and STAT3 signaling pathways. Conclusion: The phosphorylation of APP promotes the occurrence and progression of bone degenerative diseases. Psoralen regulates bone degenerative diseases by inhibiting APP phosphorylation, and regulating the MAPK and STAT3 signaling pathways.

Keywords: Psoralen, bone degenerative diseases, APP phosphorylation, MAPK, STAT3

Introduction

Bone degenerative diseases are chronic conditions affecting skeletal and joint health, including mainly osteoarthritis (OA) and osteoporosis [1, 2]. With the aging of the population, their incidence has risen significantly, posing a major public health challenge worldwide. Recent studies have revealed that the pathogenesis of bone degenerative diseases involves complex interactions among genetic, environmental, inflammatory, and metabolic factors. Among these, amyloid-β peptides (Aβ40/Aβ42) accelerate disease progression by triggering inflammatory responses, promoting extracellular matrix degradation, and inducing apoptosis. An imbalance between degradation and synthesis of the cartilage extracellular matrix is one of the core pathologic features of osteoarthritis (OA) [3]. Recent findings indicate that abnormal phosphorylation of amyloid precursor protein (APP) is a key molecular event driving chondrocyte apoptosis: phosphorylated APP significantly promotes mitochondrial dysfunction in chondrocytes by activating the caspase-3 pathway [4]. The underlying regulatory mechanism is closely associated with the MAPK/STAT3 signaling pathway. In the pathologic

https://doi.org/10.62347/YCTU6327

microenvironment of OA, persistent stimulation by inflammatory cytokines such as TNF-α and IL-1β simultaneously activates the MAPK pathway (ERK/JNK/p38) and the transcription factor STAT3. Studies have shown that phosphorylated STAT3 (p-STAT3) directly binds to the promoter region of the APP gene, increasing APP expression by 3.2-fold [5, 6]. p38 MAPK phosphorylates APP at the Thr668 site, accelerating the cleavage of APP into toxic amyloid-β peptides (Aβ), thereby creating a vicious cycle [7, 8].

Although conventional western medicine offers therapeutic effects, it is often accompanied by side effects and high recurrence rates. In contrast, natural monomers derived from traditional Chinese medicine - such as flavonoids, saponins, and alkaloids - have emerged as promising candidates for the prevention and treatment of bone degenerative diseases due to their multi-target actions, low toxicity, and favorable bioavailability [9, 10]. Their mechanisms, including anti-inflammatory, antioxidant, and bone metabolism-regulating effects, provide critical insight for developing novel diagnostic biomarkers and therapeutic strategies [11, 12]. Our previous research reported that psoralen suppresses the phosphorylation of amyloid precursor protein (APP) to inhibit myelosuppression [13]. This study focuses on psoralen, the active ingredient of the tonifying kidney prescription. Psoralen, derived primarily from the coumarin component of *Psoralea corylifolia*, possesses multiple pharmacologic effects. It exhibits protective effects against neural damage induced by Alzheimer's disease, exerting therapeutic benefits through inhibiting the formation of β-amyloid (Aβ), exhibiting anti-inflammatory properties, inhibiting neuronal apoptosis, and counteracting oxidative stress [14]. Psoralen can inhibit the proliferation and metastasis of various tumor cells *in vitro*. Its anti-inflammatory properties have been validated in models of rheumatoid arthritis, periodontitis, and airway inflammation [15]. Additionally, psoralen regulates bone homeostasis by influencing bone metabolism-related pathways, promoting osteoblast proliferation and differentiation while inhibiting osteoclast proliferation, thereby exerting an anti-osteoporotic effect.

In this study, we explored the effect of APP on degenerative diseases. We constructed the APP knockout mice, and morphologic features of the injured tissue were examined. We finally investigated the anti-osteoporotic effects and molecular mechanisms of psoralen at both animal and cellular levels.

Materials and methods

Three models of degenerative diseases (knee osteoarthritis model, osteoporosis model, and intervertebral disc degeneration model)

To meet the research requirements for degenerative diseases, we established mouse models of knee osteoarthritis (OA), osteoporosis (OP), and intervertebral disc degeneration (IVDD), and adopted simple and reliable methods to verify the success of model establishment to ensure model reliability [16-18]. The OA model was induced by anterior cruciate ligament transection (ACLT) combined with destabilization of the medial meniscus (DMM) in 8-week-old C57BL/6 mice (purchased from Shanghai Laboratory Animal Center, Chinese Academy of Sciences, Shanghai, China), and the specific construction process was as follows: All mice were fasted for 12 hours before surgery but allowed free access to water. Anesthesia was induced with 4% isoflurane (purchased from Sigma-Aldrich, St. Louis, MO, USA) mixed with medical oxygen (flow rate: 1 L/min) in an anesthesia induction box, and maintained with 1.5% isoflurane during the entire surgical process to ensure the mice remained in a stable anesthetic state. The right knee joint of each mouse was shaven and disinfected with 75% ethanol and iodophor alternately three times to avoid surgical site infection. A 0.5-0.8 cm longitudinal incision was made along the lateral side of the right knee joint, and the skin, subcutaneous tissue, and joint capsule were bluntly separated layer by layer to fully expose the anterior cruciate ligament (ACL) and medial meniscus. Under a surgical microscope (Olympus SZ61, Olympus Corporation, Tokyo, Japan), the ACL was carefully transected using micro-scissors to completely disrupt the stability of the knee joint. Subsequently, the medial meniscus was gently separated from the joint capsule, and a small section (about 1/3 of the total length) of the medial meniscus was excised to achieve medial meniscus destabilization (DMM). After confirming that the ACL was completely transected and the medial meniscus was effectively destabilized, the joint capsule was sutured with 6-0 absorbable

sutures, followed by subcutaneous tissue and skin suturing. Postoperatively, subchondral bone sclerosis was detected by micro-CT (SkyScan 1176, Bruker, Kontich, Belgium), with a threshold of >800 HU as the criterion for successful model establishment. The actual detection results showed that the subchondral bone hardness of mice after surgery was 820 ± 35 HU, all meeting the success criterion of >800 HU. Pain management was performed by subcutaneous injection of buprenorphine (purchased from MCE, Monmouth Junction, NJ, USA) at a dose of 1 mg/kg every 8 hours. Mice were placed individually on the CatWalk system (Noldus Information Technology, Wageningen, The Netherlands) to conduct daily voluntary gait monitoring without any external stimulation or restraint. Each mouse was allowed to walk freely across the glass runway until three consecutive complete, uninterrupted gait cycles were recorded. Key gait parameters including walking speed, stance phase, swing phase, and print area were automatically analyzed by the CatWalk software to evaluate pain-related gait abnormalities. Intervention was initiated promptly if the pain score reached ≥3.

The OP model was induced by ovariectomy (OVX) combined with a low-calcium diet (Ca^{2+} 0.1%, purchased from Shanghai SLAC Laboratory Animal Co., Ltd., Shanghai, China) in 12-week-old female BALB/c mice (purchased from Shanghai Laboratory Animal Center, Chinese Academy of Sciences, Shanghai, China), and the detailed construction steps were as follows: Mice were fasted for 8 hours preoperatively with free access to water. Anesthesia was induced with 4% isoflurane (Sigma-Aldrich, St. Louis, MO, USA) and maintained with 1.5% isoflurane during surgery. The dorsal skin of each mouse was shaved and disinfected with 75% ethanol and iodophor. A longitudinal incision of ≤1 cm was made at the midline of the back, 1 cm above the iliac crest. The subcutaneous fat and muscle layers were bluntly separated along the muscle fiber direction to expose the bilateral ovarian capsules. The ovarian capsule was gently torn open with micro-forceps to expose the ovary, and the ovary was separated from the surrounding connective tissue and fallopian tube. A surgical suture was used to ligate the ovarian pedicle (including blood vessels and fallopian tube) 2 mm away from the ovary, and the ovary was excised below the ligation site to ensure complete removal of ovarian tissue. The same procedure was repeated to excise the contralateral ovary. Hemostasis was achieved by electrocoagulation (electrocoagulator, Model 750, Bovie Medical Corporation, Clearwater, FL, USA) at the ligation site to prevent postoperative bleeding. After confirming no active bleeding, the muscle layer and skin were sutured sequentially with 5-0 absorbable sutures. Postoperatively, all mice were fed with a low-calcium diet (Ca^{2+} 0.1%) continuously for 8 weeks to induce osteoporosis. Eight weeks after surgery, bone mineral density of L4-L6 vertebrae was detected by DXA (Hologic Discovery W, Hologic, Inc., Bedford, MA, USA), and a reduction of ≥30% compared to the sham-operated group was regarded as the criterion for successful model establishment; mice that failed to meet this standard were excluded. The actual detection showed that the bone mineral density of L4-L6 vertebrae in mice 8 weeks after surgery was 0.18 ± 0.02 g/cm^2, which was 34.6% lower than that of the sham-operated group (0.26 ± 0.03 g/cm^2), meeting the criterion for successful model establishment. Animals were individually housed in cages (purchased from Suzhou Fengshi Laboratory Animal Equipment Co., Ltd., Suzhou, China) for 7 days after surgery with soft bedding (purchased from Shanghai SLAC Laboratory Animal Co., Ltd., Shanghai, China) provided, and euthanasia was performed immediately if pathologic fractures or >20% body weight loss occurred.

The IVDD model was established by trans-coccygeal annulus fibrosus puncture in 10-week-old CD-1 mice (purchased from Shanghai Laboratory Animal Center, Chinese Academy of Sciences, Shanghai, China), and the specific construction process is described in detail as follows: Preoperatively, mice were anesthetized with 4% isoflurane (Sigma-Aldrich, St. Louis, MO, USA) for induction and 1.5% isoflurane for maintenance, and the intraoperative core temperature was maintained at 37 ± 0.5°C using a heating pad (purchased from Harvard Apparatus, Holliston, MA, USA) to prevent hypothermia. The mouse was placed in a prone position, and the coccygeal region (Co6-Co8) was shaved and disinfected with 75% ethanol and iodophor. Under the guidance of a surgical microscope (Olympus SZ61, Olympus Corporation, Tokyo, Japan), the skin and subcutaneous tissue of the coccygeal region were bluntly separated to expose the Co7/8 intervertebral

disc. A 27G needle (purchased from BD Biosciences, Franklin Lakes, NJ, USA) was inserted vertically into the center of the Co7/8 intervertebral disc, with a puncture depth of 2 mm (controlled by a needle stopper to avoid excessive puncture injury to the nucleus pulposus). After insertion, the needle was rotated clockwise for 360° and retained for 10 seconds to fully damage the annulus fibrosus, then slowly withdrawn. After puncture, the wound was disinfected again, and no suture was required due to the small wound size. Postoperatively, enrofloxacin (purchased from MCE, Monmouth Junction, NJ, USA) (50 mg/L) was added to the drinking water 3 days pre- and post-operation to control infection. Four weeks after surgery, Pfirrmann grading was performed by MRI (3.0T MRI, Siemens, Munich, Germany), and ≥ Grade III was regarded as the criterion for successful model establishment. The actual grading results showed that 62.5% of the Co7/8 intervertebral discs in mice 4 weeks after surgery were Grade III and 37.5% were Grade IV, all meeting the requirements for successful model establishment. Motor function was monitored weekly by tail suspension test using a tail suspension device (purchased from Suzhou Fengshi Laboratory Animal Equipment Co., Ltd., Suzhou, China). All experiments were approved by the Institutional Animal Care and Use Committee of Shanghai Ruijin Hospital (IACUC-2022-028) and adhered to the 3Rs principles [14]; euthanasia was performed by gradual CO_2 asphyxiation (CO_2 gas, purchased from Shanghai Shenjiang Industrial Gases Co., Ltd., Shanghai, China) combined with cervical dislocation, in line with relevant standards [15]; all operations were performed by certified personnel in a specific pathogen-free (SPF) environment (SPF animal room, Shanghai Ruijin Hospital, Shanghai, China), and pain was evaluated using the Mouse Grimace Scale (MGS) system (purchased from Noldus Information Technology, Wageningen, The Netherlands).

Tartrate-resistant acid phosphatase (TRAP)

Bone samples underwent 24 h of fixation with 4% paraformaldehyde (PFA), 2-4 weeks of decalcification within 14% EDTA solution, paraffin embedding, and slicing into the 5-7 μm sections. Thereafter, these sections received xylene deparaffiniztion, gradient ethanol rehydration, and later incubation using the pre-warmed (37°C) TRAP staining solution supplemented with naphthol AS-BI phosphate, Fast Garnet GBC salt, and 50 mM sodium tartrate (pH 5.0) away from light for a 1-h duration. The reaction was terminated by rinsing with distilled water. Also, nuclei were counterstained with hematoxylin for 30 s, followed by mounting with neutral resin for light microscopy. The cytoplasm of osteoclasts displayed bright red granular deposits due to the enzymatic activity of TRAP, while the nuclei were stained blue. The intensity of red staining allowed us to evaluate quantitatively the osteoclast-mediated bone resorption activity.

Alcian blue staining

Samples were processed through 24 h of 4% PFA fixation, paraffin embedding, and preparation in the 5-μm sections. Afterwards, these sections received xylene deparaffiniztion, gradient ethanol rehydration, and 3 min of immersion within a 3% acetic acid solution (pH 2.5) for acidification. Then, they were further incubated with the pre-warmed (37°C) 1% Alcian blue staining solution (pH 2.5) in the dark for a 30-min duration to specifically label carboxylated glycosaminoglycans [such as hyaluronic acid (HA)]. After staining, the sections were briefly rinsed with 0.1% acetic acid, followed by 5 min of counterstaining with nuclear fast red, gradient ethanol dehydration, xylene clearing, and mounting with neutral resin. Acidic glycosaminoglycans in the cartilage matrix appeared bright blue under light microscopy, while the nuclei were stained red. The intensity of blue staining helped evaluate the distribution and abundance of proteoglycans in the cartilage matrix.

Immunofluorescence analysis

Mouse cartilage tissues (n = 6/group) were subjected to 24 h of 4% PFA fixation under 4°C, cryoprotection within 30% sucrose, and slicing into the 20 μm sections using a cryostat (Leica CM1950). The staining protocol was as follows: sections underwent permeabilization using 0.3% Triton X-100/PBS (30 min), blocking using 5% donkey serum (1 h, room temperature), and primary antibody incubation, including anti-APP (Mouse monoclonal, CST #2450, 1:200) and anti-COL12 (Rabbit polyclonal, Abcam ab65820, 1:500) for 48 h under 4°C. The sections were washed by PBS before further incubation using Alexa Fluor® 488/594-labeled

Table 1. Primer sequences

Gene	Forward Primer (5'-3')	Reverse Primer (5'-3')
APP	CAGGTGTCTGAAGGCGAATG	TGGTCACTGGTTGGTTTCGT
APH-1α	GGCTGGAACTGGTGGTCTTC	CAGCCACAGGTAGCGATGAT
PEN-2	CTGCTGGTGCTGTTCTTCCT	GGTAGGCGATGTTGTCCTTG
RAGE	GGAACCTGCCTACCTGAACG	CCTTGGCGTTCACATTCTCC
MMP3	CAAGTTTCCATTCCGCTTC	CTGGTGCAGCTCTCATATT
MMP13	ACAGTTTGTTCCTCGTGGC	CCATTCACGTCGTCCTTAT
Col2	AGGGACAGAGTCAAGTGCAG	TGGCTCTGGTCCCCAAAT
β-actin	CAGACATAGACCCAAACCCGAT	ACAGTTGCCCATTGTCAAAGAA

secondary antibodies (Invitrogen, 1:1000, 2 h, room temperature) and counterstained with DAPI. Confocal images (Zeiss LSM 880, 63× oil) were acquired under identical exposure settings. Fluorescence intensities within hippocampal CA1 regions were measured by ImageJ (v1.53). Regions of interest (ROIs) were defined, background signal was subtracted using the IgG control, and values were normalized to the DAPI-stained area.

Enzyme-linked immunosorbent assay (ELISA)

Serum was obtained in C57BL/6 mice of different ages (8, 16, and 24 weeks) by retro-orbital bleeding under isoflurane anesthesia. After centrifugation (3,000×g, 15 min, 4°C), supernatants were preserved under -80°C before use. Thereafter, amyloid-beta 40 (Aβ40), amyloid-beta 42 (Aβ42, Invitrogen, KMB3441/KMB3481), tumor necrosis factor-α (TNF-α, R&D Systems, MTA00B), and HA (Echelon Biosciences, K-1200) levels were quantified using commercial ELISA kits following manufacturers' protocols. Briefly, the 96-well plates were processed through capture antibody coating, sample or standard incubation (4°C, overnight), and subsequent detection using HRP-labeled secondary antibody (1 h, room temperature). Meanwhile, TMB substrate was used for color development, and absorbance values were read at 450 nm (SpectraMax i3x). Data analysis was completed using a 4-parameter logistic curve (GraphPad Prism 10.0), with concentrations reported in pg/mL [mean ± standard deviation (SD), n = 8/group].

Terminal deoxynucleotidyl transferase dUTP nick end labeling (TUNEL)

Cartilage tissues [osteoarthritis (OA) patients and animal models] were fixed in 4% PFA (24-48 h, 4°C), decalcified in 10% EDTA (2-4 weeks if mineralized), and paraffin-embedded. For section reparation, the 4-μm sections on poly-L-lysine slides were deparaffinized and digested using 20 μg/ml proteinase K (37°C, 30 min). Then, these sections received permeabilization with 0.1% Triton X-100/0.1% sodium citrate (ice-cold, 10 min). Afterwards, they were incubated with the TdT enzyme fluorescein-dUTP (1:9, Roche) under 37°C for 60 min, with DNase I-treated and TdT-omitted sections as controls. After PBS washes, DAPI (1 μg/ml) was added for 5 min of nuclear counterstaining.

Reverse transcription polymerase chain reaction (RT-PCR)

Total RNA from mouse cartilage and intervertebral disc tissues (n = 6/group) was isolated with TRIzol reagent (Invitrogen). RNA purity (A260/A280>1.8) and concentration were examined with NanoDrop 2000. Later, 1 μg RNA was collected to prepare cDNA with PrimeScript RT Master Mix (Takara, RR036A). The qPCR assay was carried out within the 20 μL system containing SYBR Green Premix (10 μL, Takara, RR420A), forward and reverse primers (0.4 μL, 10 μM), cDNA template (2 μL), and RNase-free water (7.2 μL). The QuantStudio 5 system was employed for amplification under conditions below: 30 s under 95°C; 5 s under 95°C and 30 s under 60°C for 40 cycles. NCBI Primer-BLAST (amplicon size: 80-150 bp) was used to design gene-specific primers (**Table 1**). Relative mRNA levels were determined via $2^{-\Delta\Delta Ct}$ approach, and GAPDH was the internal reference.

Western blot

Total protein from brain tissues and cells was isolated with ice-cold RIPA buffer (including 50 mM Tris-HCl pH 7.4, 150 mM NaCl, 1% NP-40, 0.5% sodium deoxycholate, 0.1% SDS) that contained protease/phosphatase inhibitors (containing 1 mM PMSF, 10 μg/mL aprotinin, 1 mM Na_3VO_4). Then, centrifugation (12,000×g, 4°C, 15 min) was conducted for collecting supernatants. Protein concentrations were quantified via BCA assay (Pierce™), adjusted to equivalent levels with the lysis buffer, and

denatured in the 5× Laemmli buffer (95°C, 5 min). Later, samples (20-30 μg/lane) were separated on 8-12% Tris-glycine gels (Bio-Rad) at 80 V (stacking) and 120 V (separating) using the Tris-glycine-SDS buffer, followed by transfer to activated PVDF membranes (0.45 μm, Millipore) by wet transfer (100 V, 90 min for >50 kDa proteins; 250 mA, 2 h for phosphorylated proteins). These membranes were subsequently subjected to 1 h of blocking using 5% defatted milk/TBST (for total proteins) or 5% BSA/TBST (for phosphorylated proteins) room temperature. Thereafter, they received primary antibody incubation (4°C, overnight): APP/p-APP (CST #2450/#3823, 1:1000), APH-1α (Abcam ab183591, 1:500), PEN-2 (Proteintech 12295-1-AP, 1:1000), RAGE (Abcam ab37647, 1:1000), p-p38/p38 (CST #4511/#8690, 1:2000), p-ERK1/2/ERK1/2 (CST #4370/#4695, 1:2000), p-AKT/AKT (CST #4060/#4691, 1:2000), p-STAT3/STAT3 (CST #9145/#4904, 1:2000), and β-actin (Sigma A5441, 1:5000). After washing, HRP-conjugated secondary antibodies (Jackson Lab, 1:5000) were used to conduct additional 1 h of incubation under ambient temperature. Signals were developed with SuperSignal™ substrates (Thermo) and captured by ChemiDoc™ MP. Band intensities were quantified by ImageJ (NIH), with phosphorylated proteins normalized to total counterparts and all targets to β-actin.

Statistical analysis

Results were represented as mean ± SD and tested with GraphPad Prism 9.5. The Shapiro-Wilk test was adopted to assess normality. Between-group differences were compared by unpaired Student's t-test.Among-group differences were compared by one-way ANOVA followed by the Tukey's post hoc test (for equal variances) or the Dunnett's T3 test (for unequal variances). $P<0.05$ suggested a significant difference.

Results

Changes in amyloid-beta (Aβ) and related proteins in the serum of mice at different ages

First, expression levels of Aβ40 and Aβ42 in the serum of mice at various ages (in weeks) were measured, and their concentrations were determined by ELISA. As shown in **Figure 1A**, the concentrations of Aβ40 and Aβ42 increased with the increase in the weekly mouse age. Moreover, the mRNA expression levels of amyloid precursor protein (APP), anterior pharynx defective 1 alpha (APH-1α), presenilin enhancer 2 (PEN-2), and receptor for advanced glycation end-products (RAGE) were examined through RT-PCR. Our results showed that mRNA expression of APP, APH-1α, PEN-2, and RAGE decreased as the weekly age of mice rose (**Figure 1B**). Protein levels of phosphorylated-APP (p-APP)/APP, APH-1α, PEN-2, and RAGE were examined through western blot, and our results suggested up-regulated p-APP/APP expression (**Figure 1C**). Furthermore, APH-1α, PEN-2, and RAGE had reduced protein levels with increasing weekly age of mice (**Figure 1C**).

Expression levels of Aβ peptide and its associated proteins in three models of bone degenerative diseases

The levels of Aβ peptide and its related molecules in serum were detected by ELISA. According to the results, there were significant increases in the contents of Aβ40 and Aβ42 in three models of bone degenerative diseases, namely, the knee osteoarthritis model, the osteoporosis model, and the intervertebral disc degeneration model (**$P<0.01$, **Figure 2A**). We conducted RT-PCR assay for measuring mRNA levels of APP as well as upstream and downstream targets (APH-1α, PEN-2, RAGE). As discovered, mRNA levels of the above proteins markedly decreased in these three models of bone degenerative diseases (**$P<0.01$, **Figure 2B**, **2C**).

p-APP and APP, along with upstream and downstream proteins (APH-1α, PEN-2, RAGE) were then assessed through western blot. As discovered, in the three models of bone degenerative diseases mentioned above, the p-APP levels increased, while APP, APH-1α, PEN-2, and RAGE proteins had significantly decreased levels (**Figure 2D**).

Further, immunofluorescence analysis was performed for investigating APP expression and distribution in the tissues. The results revealed that in the three models of bone degenerative diseases, the levels of APP significantly decreased, and the distribution range was significantly expanded (**Figure 3**).

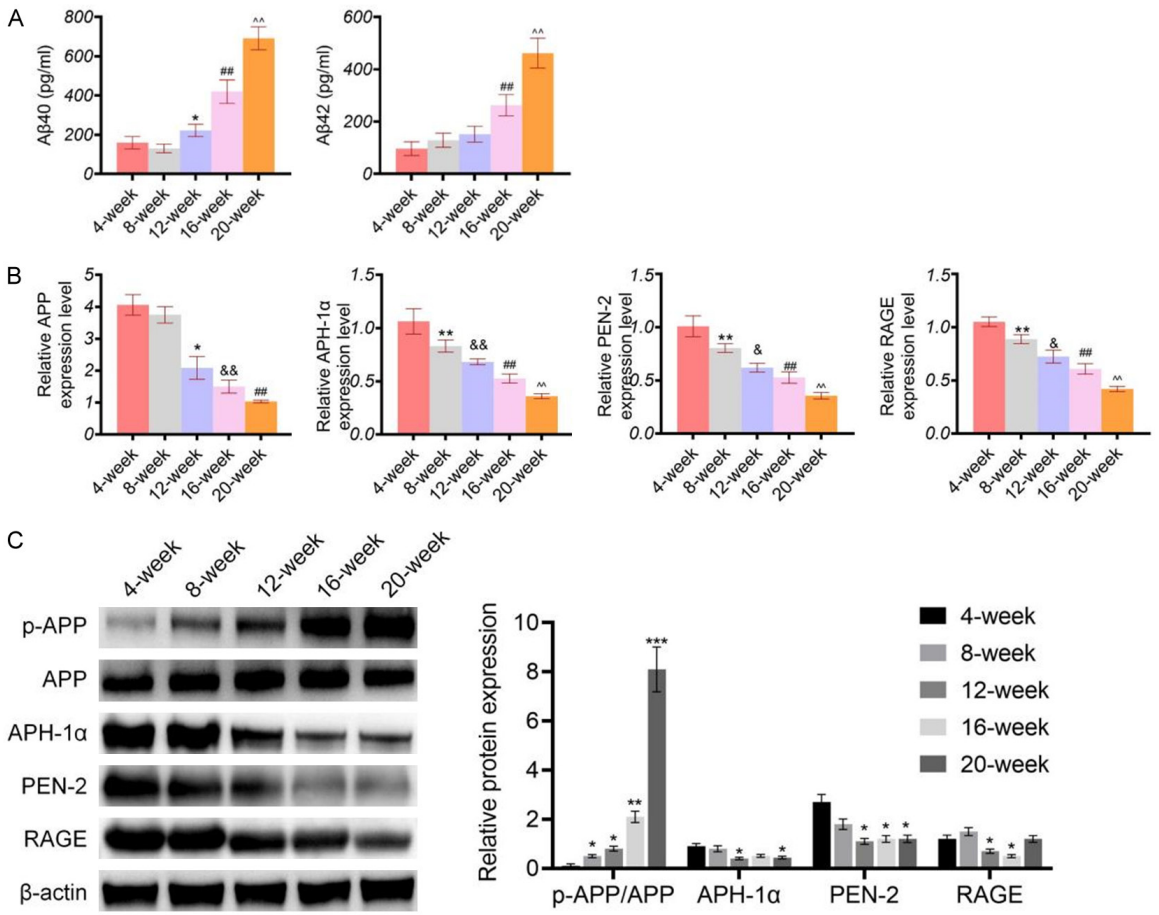

Figure 1. Changes in Aβ and related proteins in serum of mice at different ages. A. The expression of Aβ40 and Aβ42 in the serum of mice at different ages was detected by ELISA. **P*<0.05 vs 4-week group, $^{\&}$*P*<0.05, $^{\&\&}$*P*<0.01 vs 8-week group, $^{\#\#}$*P*<0.01 vs 12-week group, ^^*P*<0.01 vs 16-week group. B. The mRNA expression of APP, APH-1α, PEN-2, and RAGE in serum of mice at different ages were examined by RT-PCR. **P*<0.05, ***P*<0.01 vs 4-week group, $^{\&}$*P*<0.05, $^{\&\&}$*P*<0.01 vs 8-week group, $^{\#\#}$*P*<0.01 vs 12-week group, ^^*P*<0.01 vs 16-week group. C. The protein expression of p-APP/APP, APH-1α, PEN-2, and RAGE in serum of mice at different ages was also examined by western blot. **P*<0.05, ***P*<0.01, ****P*<0.0001 vs 4-week group. Data were shown as mean ± SD.

APP knockout significantly accelerates the progression of degenerative changes in mice

Subsequently, an APP knockout mouse model was established. As indicated by PCR and western blot assays, both APP mRNA and protein levels in APP knockout mice were significantly reduced compared with normal mice (**Figure 4A**), confirming the successful establishment of the APP knockout mouse model. Moreover, Safranin O staining results demonstrated that, compared to normal mice, the degree of osteoarthritis in the knee joints of APP knockout mice increased significantly with age (**Figure 4B**). This finding suggests that APP knockout may promote the occurrence of degenerative changes in mice. Besides, ELISA analysis on serum TNF-α and HA contents revealed that, relative to normal mice, serum TNF-α and HA contents in APP knockout mice increased significantly with age (**Figure 4C**). These results further support the hypothesis that APP knockout significantly promotes inflammation during the progression of degenerative changes in mice.

Immunohistochemistry (IHC) was employed to count the number of osteoclasts (TRAP-positive) in vertebral bodies. Compared to normal mice, APP knockout mice had increased osteoclast number (TRAP-positive) with age (**Figure 4D**). Moreover, intervertebral disc degeneration was assessed using H&E staining, and the results indicated that, relative to nor-

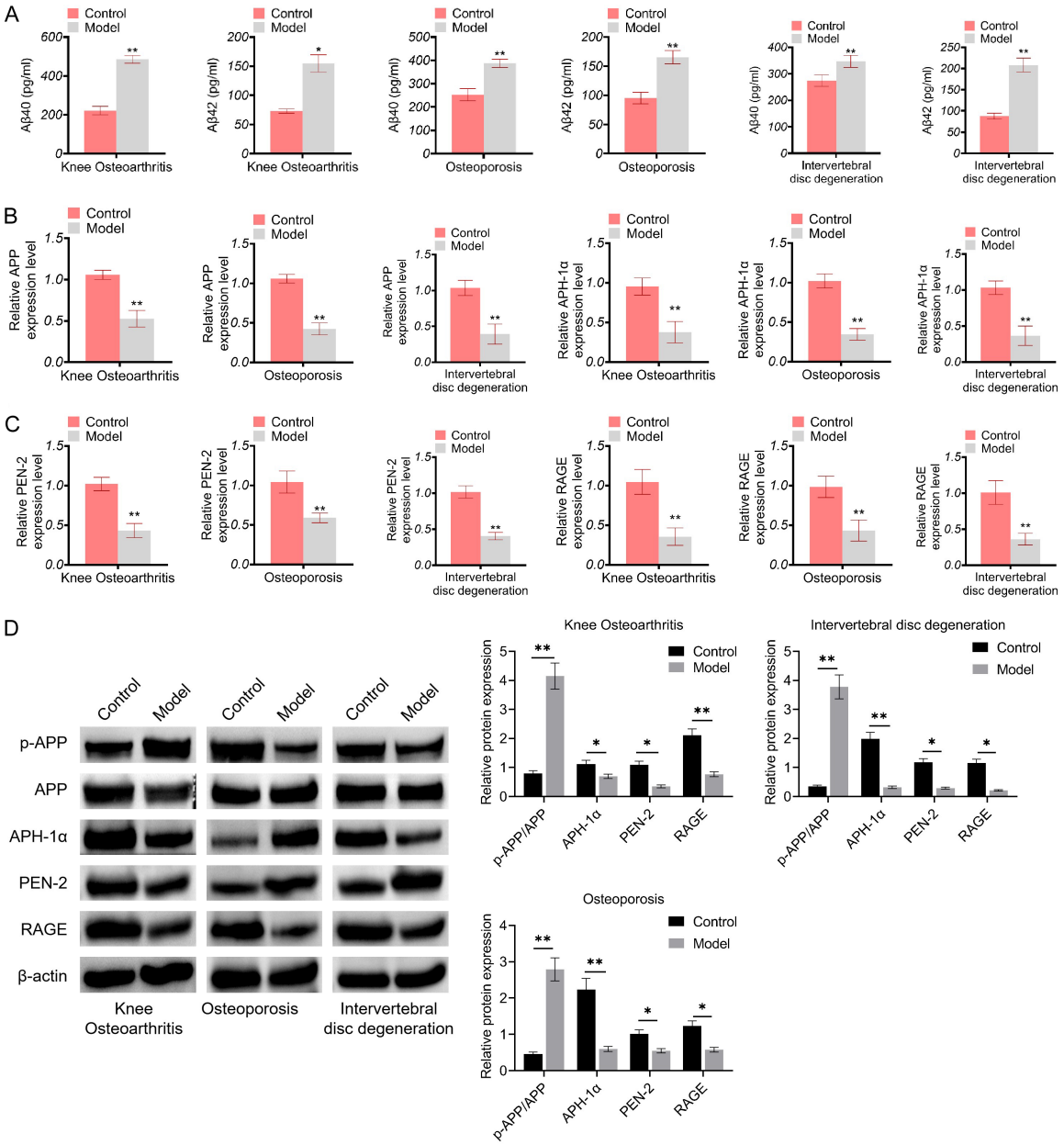

Figure 2. Expression of Aβ peptide and its associated proteins in three models of bone degenerative diseases. A. The knee osteoarthritis model, the osteoporosis model, and the intervertebral disc degeneration model were constructed. B. The expression of Aβ40 and Aβ42 in the serum of mice with bone degenerative diseases was detected by ELISA. C. The APP mRNA and the mRNA expression of upstream and downstream targets (APH-1α, PEN-2, RAGE) in the serum of mice with bone degenerative diseases was examined by RT-PCR. D. The protein expression of p-APP/APP and upstream/downstream proteins (APH-1α, PEN-2, RAGE) was assessed by western blot. Data were shown as mean ± SD. **P*<0.05, ***P*<0.01 vs control group.

mal mice, the process of intervertebral disc degeneration was accelerated in APP knockout mice as they aged (**Figure 4E**). Immunofluorescence staining was also carried out to analyze the level of type II collagen (Col2) within the intervertebral discs. Compared to normal mice, APP knockout mice exhibited a significant decrease in the level of Col2 within their intervertebral discs with age (**Figure 5**).

TUNEL staining was conducted for counting apoptotic cell number in the intervertebral disc. As suggested by the results, compared to normal mice, APP knockout mice displayed a sig-

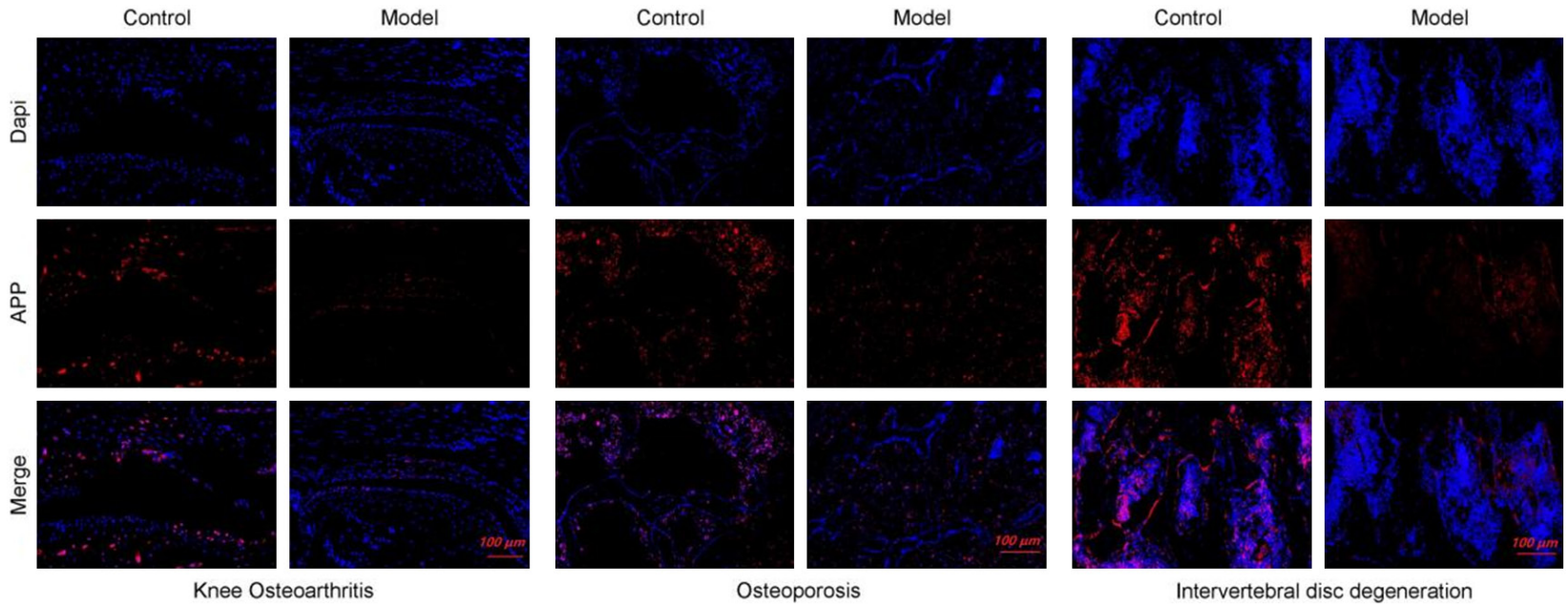

Figure 3. Expression of APP in bone tissues. The expression and distribution of APP in the bone tissues of three models of degenerative diseases was conducted by immunofluorescence. Scale bar: 100 μm, ×100 magnification.

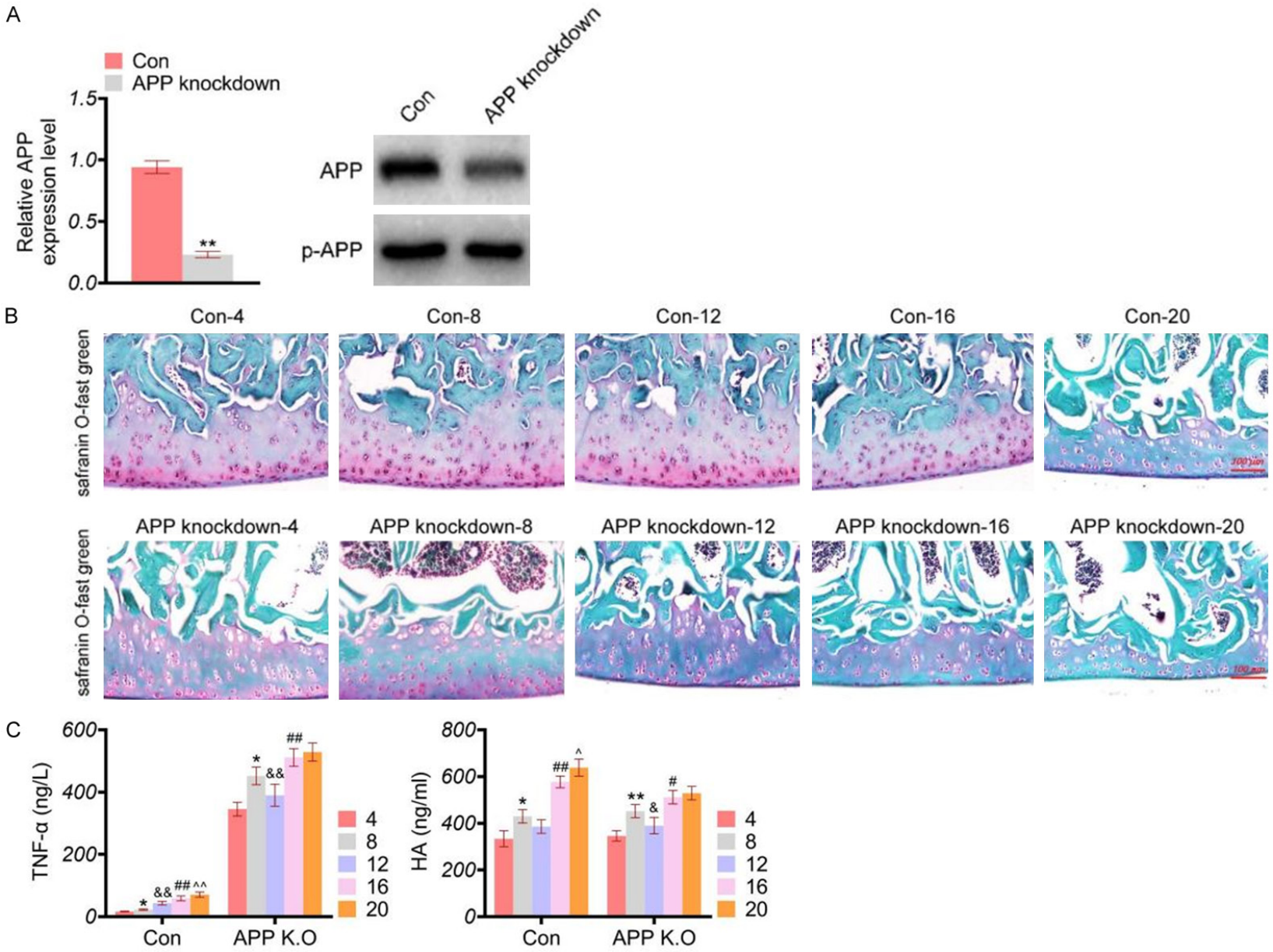
A
Con
APP knockdown
Relative APP expression level
1.5
1.0
0.5
0.0
**
Con
APP knockdown
APP
p-APP
B
Con-4
Con-8
Con-12
Con-16
Con-20
safranin O-fast green
APP knockdown-4
APP knockdown-8
APP knockdown-12
APP knockdown-16
APP knockdown-20
safranin O-fast green
C
TNF-α (ng/L)
600
400
200
0
Con
APP K.O
4
8
12
16
20
HA (ng/ml)
800
600
400
200
0
Con
APP K.O
4
8
12
16
20

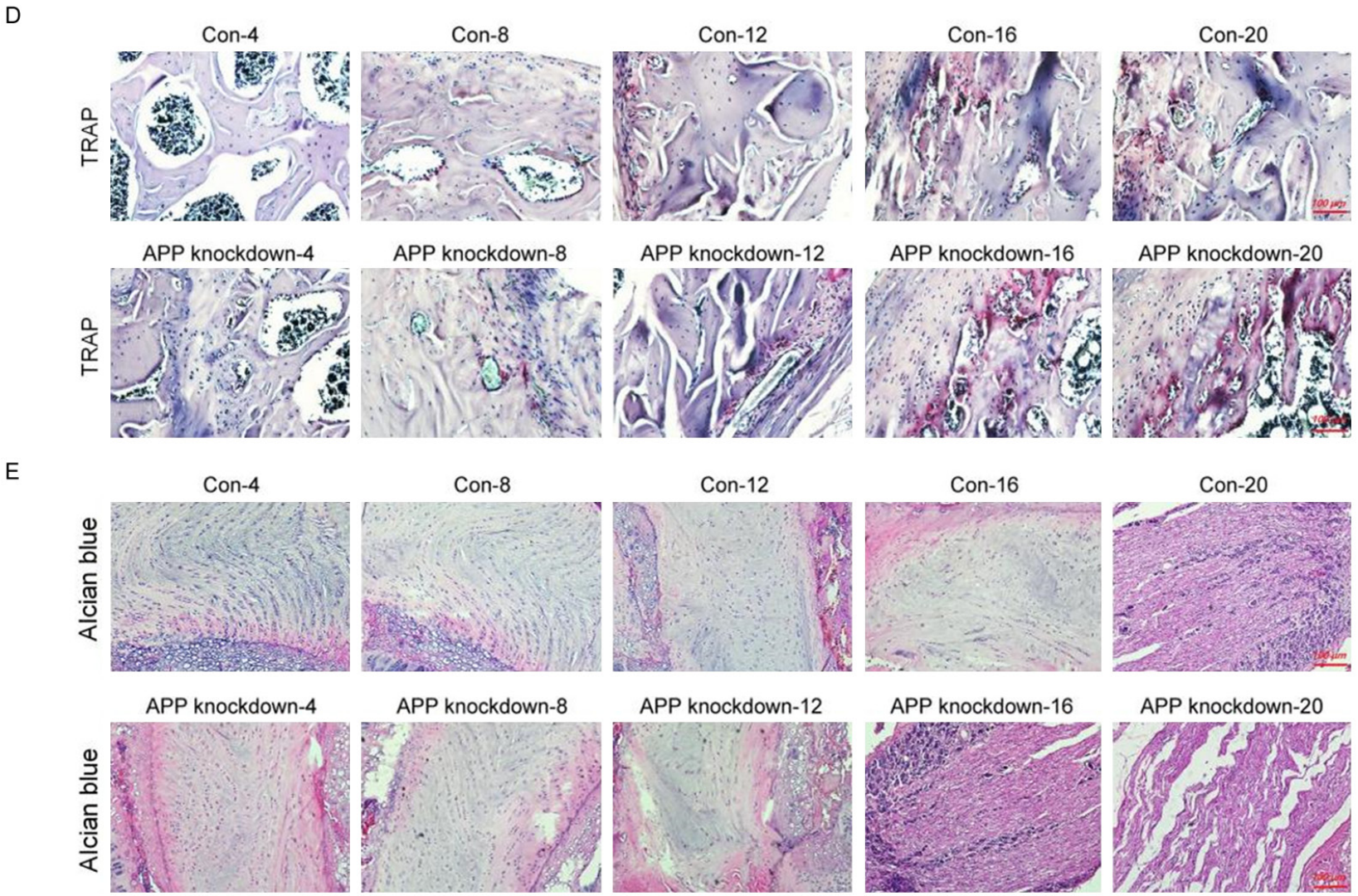

Figure 4. Knockout of APP significantly accelerated the progression of degenerative changes in mice. A. The protein expression of APP in bone tissues was examined by western blot. $^{**}P<0.01$ vs controls. B. Safranin O staining was performed to detect the bone tissue morphology. C. The levels of TNF-α and HA in control and APP knockout mice serum were tested by ELISA. $^{*}P<0.05$, $^{**}P<0.01$ vs 4-week group; $^{\&}P<0.05$, $^{\&\&}P<0.01$ vs 8-week group; $^{\#}P<0.05$, $^{\#\#}P<0.01$ vs 12-week group; $^{\wedge\wedge}P<0.01$ vs 16-week group. D. The IHC method was used to count the number of osteoclasts (TRAP-positive) in vertebral bodies. E. H&E staining was used for the assessment of intervertebral disc degeneration. Data were shown as mean ± SD. $^{*}P<0.05$, $^{**}P<0.01$ vs 4-week group, $^{\&\&}P<0.01$ vs 8-week, $^{\#\#}P<0.01$ vs 12-week, $^{\wedge\wedge}P<0.01$ vs 16-week. Scale bar: 100 μm, ×100 magnification.

nificant increase in the cell apoptosis level within the intervertebral discs as they aged (**Figure 6A**). These findings demonstrate that APP knockout can significantly promote the progression of degenerative diseases in mice. RT-PCR assay was performed to assess the mRNA expression of matrix metalloproteinase 3 (MMP3), matrix metalloproteinase 13 (MMP-13), and Col2 in intervertebral discs. From our observations, relative to normal mice, APP knockout mice exhibited an apparent decrease in MMP3 mRNA level, a notable increase in MMP13 mRNA level, and a remarkable decrease in Col2 mRNA level within their intervertebral discs as they aged in weeks (**Figure 6B**).

Psoralen regulates bone degenerative diseases by inhibiting APP phosphorylation and cell apoptosis in mice

We further constructed an osteoporosis model and intervened in this animal model with varying concentrations of psoralen (low, medium, and high dose groups). IHC analysis was conducted to count the number of osteoclasts (TRAP-positive) in the vertebral bodies. As a result, intervention with psoralen at different concentrations (low, medium, and high dose groups) markedly decreased the TRAP-positive osteoclast number in vertebral bodies of mice with osteoporosis, with a higher dose yielding a more pronounced effect (**Figure 7A**). In addition, we conducted RT-PCR for detecting mRNA levels of APP and its upstream and downstream molecules (APH-1α, PEN-2, RAGE). The results revealed that after intervention with psoralen at different concentrations (low, medium, and high dose groups) in the osteoporosis animal model, the mRNA levels of APP and its upstream and downstream molecules (APH-1α, PEN-2, RAGE) markedly increased dose-dependently (**Figure 7B**). Western blot assay was used to detect levels of APP, p-APP, and upstream and downstream proteins (APH-1α, PEN-2, RAGE). After intervention with different concentrations of psoralen (low, medium, and high dose groups) in the osteoporosis model, the expression levels of APP as well as upstream and downstream proteins were significantly reduced, with better effects achieved at higher doses (**Figure 7C**). Further, proteins associated with signaling pathways and their phosphorylated forms [phosphorylated-p38 (p-p38)/mitogen-activated protein kinase (p38), phosphorylated-ERK1/2 (p-ERK1/2)/extracellular signal-regulated kinase 1/2 (ERK1/2), phosphorylated-AKT (p-AKT)/protein kinase B (AKT), phosphorylated-STAT (p-STAT3)/signal transducer and activator of transcription 3 (STAT3)] were also quantified by western blot. Notably, the MAPK pathway promotes osteogenic differentiation, the AKT pathway enhances osteogenic differentiation, and STAT3 also facilitates osteogenic differentiation. From our results, following intervention with different concentrations of psoralen (low, medium, and high dose groups) in the osteoporosis animal model, p-p38, p-AKT, and p-STAT3 (key proteins involved in the three pathways that promote bone differentiation) levels markedly increased (**Figure 7D**). These findings suggest that psoralen can significantly ameliorate degenerative changes in mice in a dose-dependent manner.

Psoralen significantly ameliorates degenerative changes at the cellular level

Finally, we intervened with psoralen in osteoblasts and assessed the proliferation of the MC3T3-E1 osteoblasts by Cell Counting Kit-8 (CCK8) assay. As a result, after treating osteoblasts with different concentrations of psoralen (low, medium, and high dose groups), cell viability increased significantly, and a superior efficacy was achieved at a higher dose (**Figure 8A**). PCR assay of Runt-related transcription factor 2 (Runx2) and osteocalcin mRNA levels revealed that after osteoblasts were exposed to psoralen treatment at varying concentrations (low, medium, and high dose groups), mRNA levels of Runx2 and osteocalcin increased dramatically (**Figure 8B**). Moreover, western blot assay of the phosphorylation status of related pathway proteins indicated that after osteoblasts were exposed to psoralen treatment at varying concentrations (low, medium, and high dose groups), p-p38, p-AKT, and p-STAT3 had remarkably increased levels (**Figure 8C**). These results demonstrate that psoralen can significantly ameliorate degenerative changes in osteoblasts at the cellular level dose-dependently.

Following intervening with psoralen in osteoblasts, the cells were further treated with MAPK inhibitor (SB203580), AKT inhibitor (LY294002), and STAT3 inhibitor (WP1066). Subsequently, we carried out CCK8 assay for detecting the

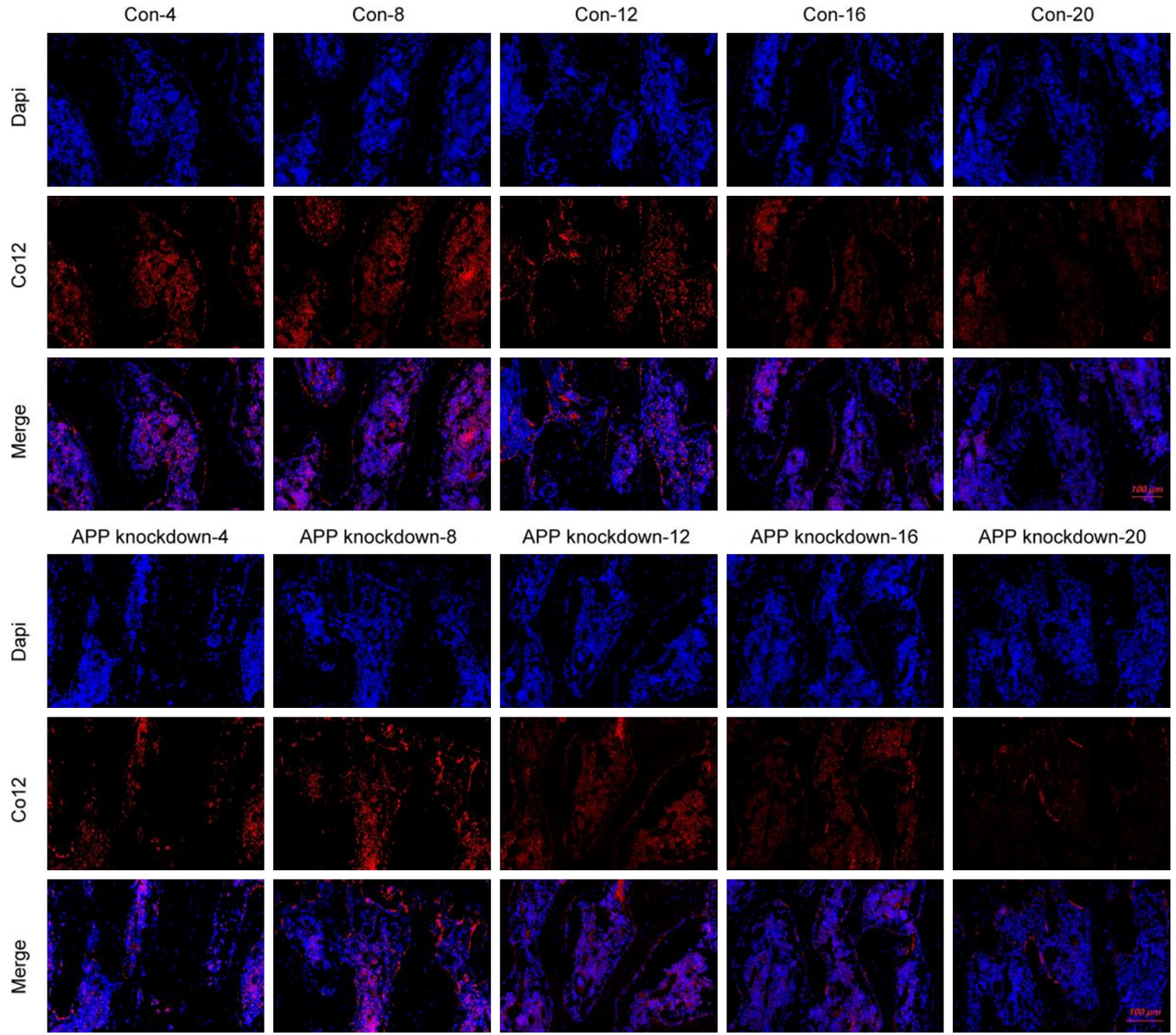
Con-4
Con-8
Con-12
Con-16
Con-20
Dapi
Co12
Merge
100 μm
APP knockdown-4
APP knockdown-8
APP knockdown-12
APP knockdown-16
APP knockdown-20
Dapi
Co12
Merge
100 μm

Figure 5. The level of Col2 in intervertebral discs in control and APP knockout mice at different ages. Immunofluorescence staining was used to analyze the level of Col2 within the intervertebral discs. Scale bar: 100 μm, ×100 magnification.

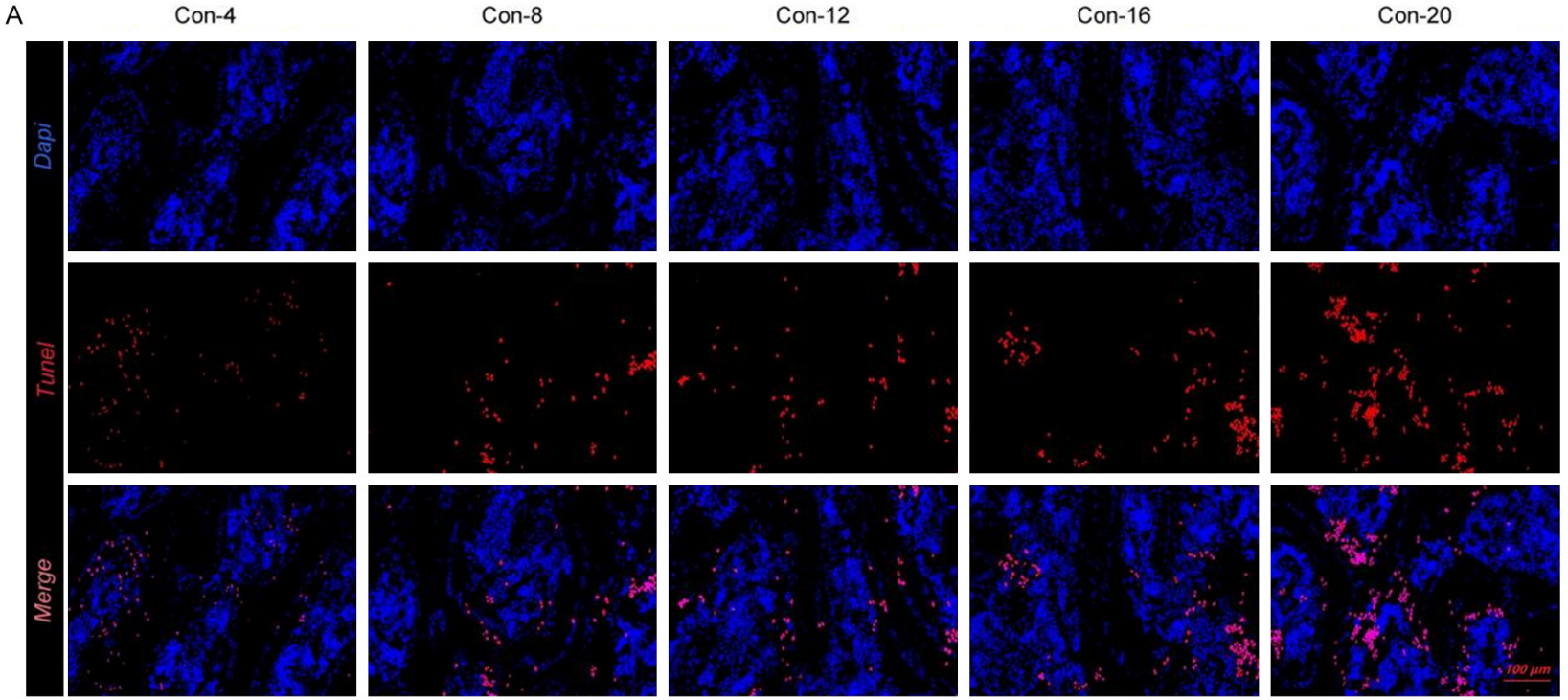

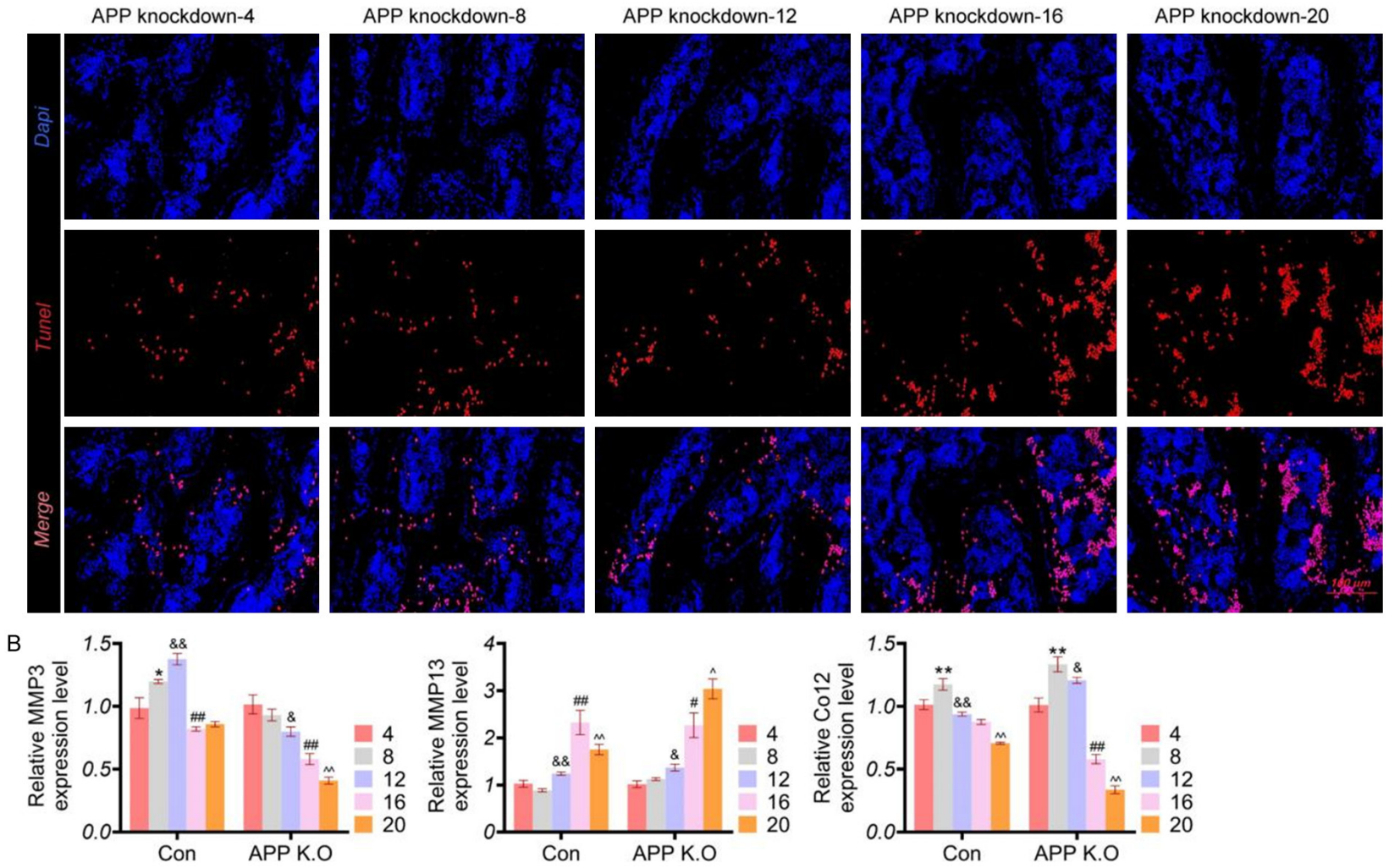

Figure 6. The apoptotic cells, MMP3, MMP13, and Col2 expressions in the intervertebral disc in control and APP knockout mice at different ages. A. TUNEL staining was used to analyze the number of apoptotic cells in the intervertebral disc. B. The MMP3, MMP13 and Col2 expression levels were assessed by ELISA. Data were shown as mean ± SD. **P*<0.05, ***P*<0.01 vs 4-week group; $^{\&}P$<0.05, $^{\&\&}P$<0.01 vs 8-week group; $^{\#}P$<0.05, $^{\#\#}P$<0.01 vs 12-week group; ^*P*<0.05, ^^*P*<0.01 vs 16-week group. Scale bar: 100 μm, ×100 magnification.

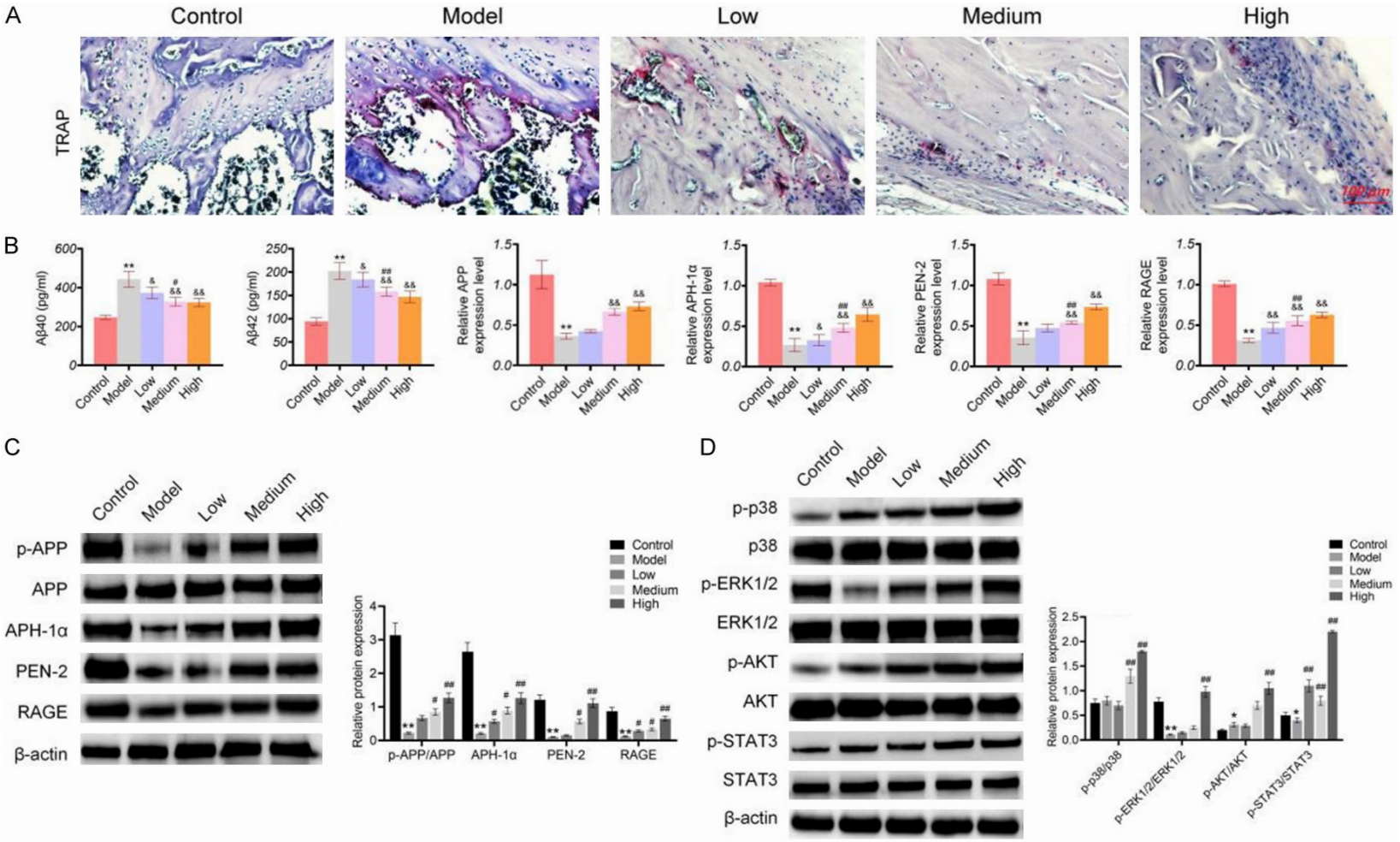

Figure 7. Psoralen regulates bone degenerative diseases by inhibiting APP phosphorylation, MAPK, AKT, and STAT3 signaling. A. We further developed an osteoporosis model and intervened in this animal model with varying concentrations of psoralen (low, medium, and high dose groups). Immunohistochemical staining was done to count the number of osteoclasts (TRAP-positive) in the vertebral bodies. B. RT-PCR was performed to detect the mRNA expression of APP, APH-1α, PEN-2, and RAGE. C. Western blot analysis was conducted to detect the protein expression levels of APP, phosphorylated APP, APH-1α, PEN-2, and RAGE. D. Western blot was also used to assess the expression of proteins related to signaling pathways and their phosphorylated forms (p-p38/p38, p-ERK1/2/ERK1/2, p-AKT/AKT, p-STAT3/STAT3). Data were shown as mean ± SD. **P*<0.05, ***P*<0.01 vs Control group; $^{\&}P$<0.05, $^{\&\&}P$<0.01 vs Model group. Scale bar: 100 μm, ×100 magnification.

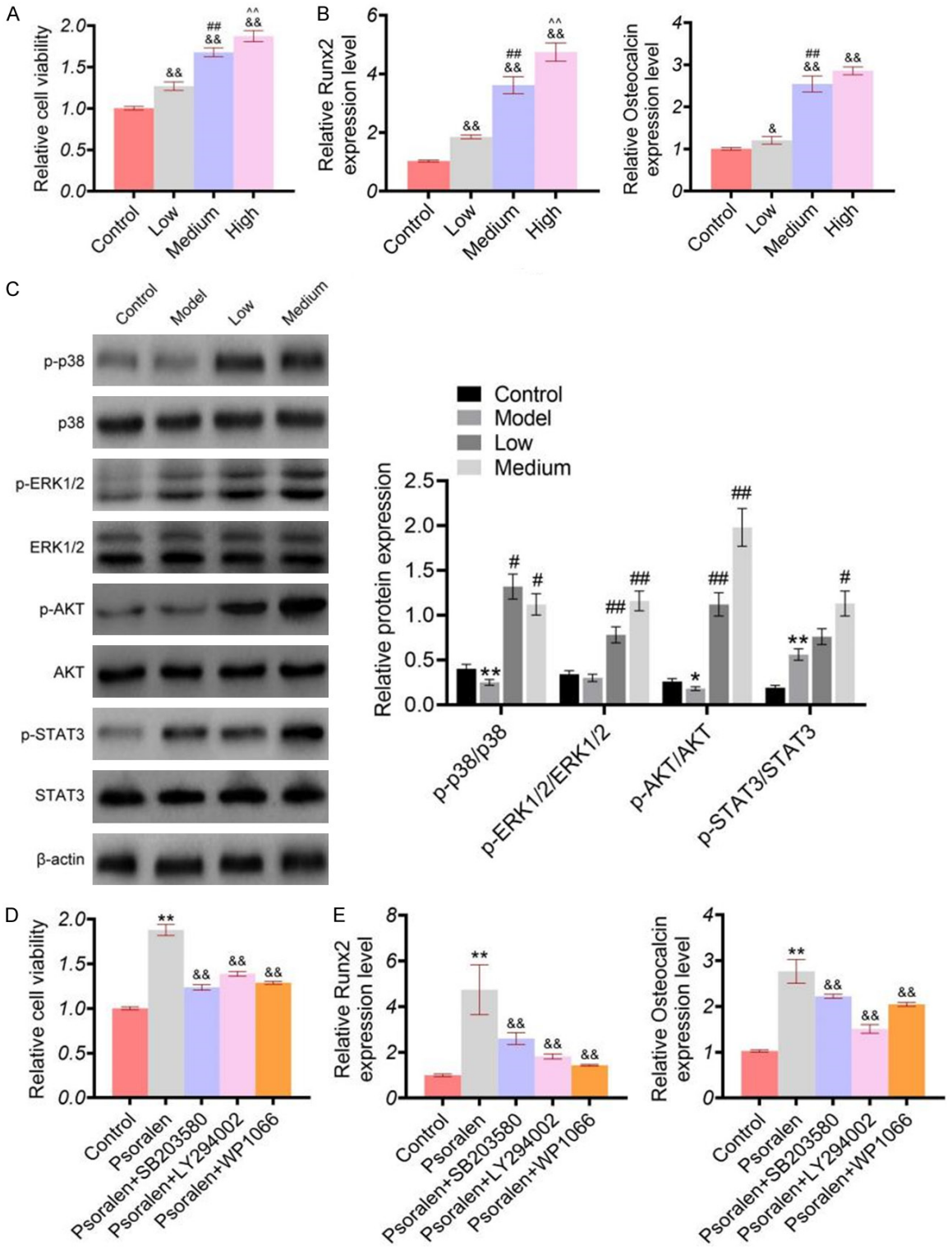

Figure 8. Psoralen significantly ameliorated degenerative changes at the cellular level. A. Osteoblasts MC3T3-E1 were exposed to psoralen and the proliferation level was assessed using the CCK8 assay. $^{\&\&}P<0.01$ vs Control group, $^{\#\#}P<0.01$ vs Low group, $\wedge\wedge P<0.01$ vs Medium group. B. The Runx2 and osteocalcin mRNA levels were examined by RT-PCR. $^{\&\&}P<0.01$ vs Control group, $^{\#\#}P<0.01$ vs Low group, $\wedge\wedge P<0.01$ vs Medium group. C. Western blot was performed to examine the phosphorylation status of related pathway proteins. $^{*}P<0.015$, $^{**}P<0.01$ vs Control group; $^{\#}P<0.05$, $^{\#\#}P<0.01$ vs Model group. D. After exposure to psoralen in osteoblasts, the cells were further treated with MAPK inhibitor (SB203580), AKT inhibitor (LY294002), and STAT3 inhibitor (WP1066). CCK8 assay was conducted to detect the proliferation level of osteoblasts MC3T3-E1. $^{**}P<0.01$ vs Control group, $^{\&\&}P<0.01$ vs Psoralen group. E. PCR analysis of Runx2 and osteocalcin mRNA levels was performed. $^{**}P<0.01$ vs Control group, $^{\&\&}P<0.01$ vs Psoralen group. Data were shown as mean ± SD.

MC3T3-E1 osteoblast proliferation. After blocking the signaling pathways with MAPK inhibitor (SB203580), AKT inhibitor (LY294002), and STAT3 inhibitor (WP1066), the viability of MC3T3-E1 osteoblasts was significantly reduced compared to the psoralen-treated group (**Figure 8D**). Additionally, PCR assay of Runx2 and osteocalcin mRNA levels revealed that after blocking the signaling pathways with these inhibitors, Runx2 and osteocalcin had markedly down-regulated mRNA levels in osteoblasts relative to the psoralen-treated group (**Figure 8E**). Collectively, these observations illustrate that the mechanism by which psoralen ameliorates degenerative changes in mice may be mediated through the MAPK, AKT, and STAT3 signaling pathways.

Discussion

This study first reveals the pathological association between APP phosphorylation and bone degenerative diseases, demonstrating that psoralen exerts multi-target regulatory effects on delaying disease progression. Recently, notable advancement has been achieved in psoralen research concerning bone metabolic disorders and neurodegenerative diseases. Studies have reported that cyclophosphamide impairs osteogenic differentiation of bone marrow stromal cells (BMSCs) through suppressing Wnt/β-catenin pathway, while 200 μmol/L psoralen effectively reverses this damage by specifically activating the Wnt4/β-catenin axis. This offers a strategy for preventing chemotherapy-associated osteoporosis [19, 20]. Nevertheless, its photosensitivity and hepatotoxicity risks necessitate optimized delivery systems to enhance safety. Recent investigations have further identified the inhibitory effects of psoralen derivatives on breast cancer and drug-resistant bacteria, opening new avenues for multi-target drug development.

Our experimental data showed that p-APP expression increased with aging in mice, accompanied by an abnormal Aβ42/Aβ40 ratio (detected by ELISA). Meanwhile, APP knockout mice developed progressive bone degenerative pathologies, as evidenced by the loss of cartilage matrix via Safranin O staining and the increase in osteoclasts in vertebral bodies. This parallels the mechanism in Alzheimer's disease (AD) where aberrant APP cleavage leads to Aβ deposition, suggesting that C-terminal fragments (CTFs) of APP may activate osteoclast differentiation signaling via RAGE receptors while suppressing the MAPK/AKT pathway activity in osteoblasts (as evidenced by the down-regulated APH-1α and PEN-2 mRNA levels in RT-PCR). This provides novel evidence for the shared mechanisms between bone metabolic disorders and neurodegenerative diseases. Intervention with psoralen confers dose-dependent protection: (1) At the animal level, it significantly reduces serum TNF-α levels ($P<0.01$) and elevates HA content, ameliorating intervertebral disc degeneration (revealed by annulus fibrosus structural repair in H&E staining); (2) At the cellular level, it accelerates osteoblast proliferation (verified through CCK-8 assay) and inhibits STAT3 phosphorylation (validated by western blot), aligning with its previously reported suppression of RANKL-induced osteoclastogenesis. Notably, co-administration with MAPK and AKT inhibitors partially counteracts the role of psoralen in increasing Col2 expression, indicating its dual-pathway mechanism-directly inhibiting APP cleavage and indirectly modulating the inflammation-osteogenesis coupling network-in maintaining bone microenvironment homeostasis. Although psoralen exhibits efficacy across the three bone disease models (osteoarthritis, osteoporosis, and intervertebral disc degeneration), its limited blood-brain barrier permeability may restrict central modulation of the APP pathway. Future studies should optimize delivery methods (e.g., nanocarrier-targeted systems) and explore synergies with anti-osteoporotic drugs like bisphosphonates. Moreover, the biomarker value of Aβ42/Aβ40 ratio for bone metabolic disorders requires further validation in larger clinical cohorts. Nonetheless, there are certain limitations to be noted in this study. First, the current research only utilized mouse models, whose bone metabolism characteristics are different from humans, and did not consider special pathologic conditions such as postmenopausal osteoporosis. Second, although the involvement of MAPK/AKT/STAT3 pathways in the regulatory mechanisms was confirmed, the direct interaction target between psoralen and APP phosphorylation remains unidentified. Third, human pharmacokinetic data and long-term medication safety evaluations are lacking. In our future research, we will establish humanized APP transgenic mouse and organoid models, validate the cross-spe-

cies efficacy of psoralen based on clinical samples, screen the psoralen-APP complexes via proteomics and elucidate binding sites through molecular dynamic simulations, and evaluate the synergistic effects between psoralen and existing anti-osteoporosis agents.

Collectively, the present work illustrates the novel mechanism of psoralen in regulating bone degenerative diseases by the MAPK/STAT3/APP axis, providing a theoretical basis for developing natural drugs targeting APP phosphorylation. Future studies should focus on the structural modifications of psoralen to enhance targeting specificity and pursue individualized therapeutic strategies based on Aβ dynamic monitoring.

Acknowledgements

This work was supported by Youth Science Foundation Project of National Natural Science Foundation of China (81603637), General projects of Shanghai Natural Science Foundation (20ZR1433800), Shanghai Sailing Program (20YF1427400), Shanghai Traditional Chinese Medicine Association "KaiBao" Youth Physician Inheritance Research Project of Shanghai-Style Traditional Chinese Medicine (2023-HPZY-05), and Shanghai Flagship Hospital of Integrated Traditional Chinese and Western Medicine Construction Program [ZY (2021-2023)-0205-01].

Disclosure of conflict of interest

None.

Address correspondence to: Dr. Youji Jia, Department of Traumatology, Shanghai Ruijin Hospital, Shanghai Jiao Tong University School of Medicine, Shanghai 200025, China. E-mail: jiayouji0115@163.com; Dr. Xiaobing Xi, Shanghai Key Laboratory for Bone and Joint Diseases, Shanghai Institute of Traumatology and Orthopaedics, Shanghai Ruijin Hospital, Shanghai Jiao Tong University School of Medicine, Shanghai 200025, China. E-mail: skxixiaobing@163.com

References

[1] Endo Y. Editorial: from crosstalk among cell populations in the microenvironment of bone degenerative diseases to the novel therapeutic approaches. Front Med (Lausanne) 2026; 13: 1812496.

[2] Pang Y, Zhu S, Xu J, Su C, Wu B, Zhang C and Gao J. Myeloid cells as a promising target for brain-bone degenerative diseases from a metabolic point of view. Adv Biol (Weinh) 2023; 7: e2200321.

[3] Kalvaityte U, Matta C, Bernotiene E, Pushparaj PN, Kiapour AM and Mobasheri A. Exploring the translational potential of clusterin as a biomarker of early osteoarthritis. J Orthop Translat 2021; 32: 77-84.

[4] Nguyen JP, Dixneuf V, Esnaut J, Moreno AS, Malineau C, Nizard J and Lefaucheur JP. The value of high-frequency repetitive transcranial magnetic stimulation of the motor cortex to treat central pain sensitization associated with knee osteoarthritis. Front Neurosci 2019; 13: 388.

[5] Chen Y, Deng Q, Wang C, Liang C, Shi Y, Liu X, Deng C, Li J, Zhang H and Hua Q. Investigation of cognitive enhancements and mechanisms of kinsenoside in app/ps1 mice through network pharmacology, in vivo experiments, and machine learning. Life Sci 2025; 378: 123810.

[6] Long QH, Wu YG, He LL, Ding L, Tan AH, Shi HY and Wang P. Suan-zao-ren decoction ameliorates synaptic plasticity through inhibition of the aβ deposition and jak2/stat3 signaling pathway in ad model of app/ps1 transgenic mice. Chin Med 2021; 16: 14.

[7] Li C, Wang L, Xie W, Chen E, Chen Y, Li H, Can D, Lei A, Wang Y and Zhang J. Tgr5 deficiency in excitatory neurons ameliorates alzheimer's pathology by regulating app processing. Sci Adv 2024; 10: eado1855.

[8] Mehla J, Singh I, Diwan D, Nelson JW, Lawrence M, Lee E, Bauer AQ, Holtzman DM and Zipfel GJ. Stat3 inhibitor mitigates cerebral amyloid angiopathy and parenchymal amyloid plaques while improving cognitive functions and brain networks. Acta Neuropathol Commun 2021; 9: 193.

[9] Li C, Lin X, Lin Q, Lin Y and Lin H. Jiangu granules ameliorate postmenopausal osteoporosis via rectifying bone homeostasis imbalance: a network pharmacology analysis based on multi-omics validation. Phytomedicine 2024; 122: 155137.

[10] Gu S, Wang J, Yu S, Zhang S, Gao T, Yan D, Xie R, Gu M, Yu M, Zhang Z, Lou Z, Ding X, Chen Y and Li C. Berberine ameliorates nonalcoholic fatty liver disease-induced bone loss by inhibiting ferroptosis. Bone 2024; 185: 117114.

[11] Lin S, Song D, Wang S, Song Z, Xing F, Hong Z, Luo J, Song Q, Fang Z, Chen XC, Lu YJ and Jin F. Nuanxin formula inhibits bone resorption to combat osteoporosis by attenuating osteoclast oxidative phosphorylation. J Ethnopharmacol 2025; 350: 119998.

[12] Li Y and Li F. Mechanism and prospect of gastrodin in osteoporosis, bone regeneration, and osseointegration. Pharmaceuticals (Basel) 2022; 15: 1432.
[13] Jia Y, Wang G, Yan W, Kong B, Xu Y, Wang C, Tang D and Xi X. Psoralen suppresses the phosphorylation of amyloid precursor protein (app) to inhibit myelosuppression. Biomed Pharmacother 2022; 153: 113381.
[14] Tripathi N, Bhardwaj N, Kumar S and Jain SK. Phytochemical and pharmacological aspects of psoralen - a bioactive furanocoumarin from psoralea corylifolia linn. Chem Biodivers 2023; 20: e202300867.
[15] Wang K, Yin C, Ye X, Chen Q, Wu J, Chen Y, Li Y, Wang J, Duan C, Lu A and Guan D. A metabolic driven bio-responsive hydrogel loading psoralen for therapy of rheumatoid arthritis. Small 2023; 19: e2207319.
[16] Hall M, van der Esch M, Hinman RS, Peat G, de Zwart A, Quicke JG, Runhaar J, Knoop J, van der Leeden M, de Rooij M, Meulenbelt I, Vliet Vlieland T, Lems WF, Holden MA, Foster NE and Bennell KL. How does hip osteoarthritis differ from knee osteoarthritis? Osteoarthritis Cartilage 2022; 30: 32-41.
[17] Li Y, Gao H, Zhao L and Wang J. Osteoporosis in copd patients: risk factors and pulmonary rehabilitation. Clin Respir J 2022; 16: 487-496.
[18] Samanta A, Lufkin T and Kraus P. Intervertebral disc degeneration-current therapeutic options and challenges. Front Public Health 2023; 11: 1156749.
[19] Manolagas SC. Wnt signaling and osteoporosis. Maturitas 2014; 78: 233-237.
[20] Formosa MM, Christou MA and Mäkitie O. Bone fragility and osteoporosis in children and young adults. J Endocrinol Invest 2024; 47: 285-298.